The Role of 1D and 3D Radiative Heating on the Organization of Shallow Cumulus Convection and the Formation of Cloud Streets

Jakub Fabian[1] and Mayer Bernhard[1]

[1]Meteorological Institute, Ludwig Maximilian Universität München, LMU

Correspondence to: Jakub Fabian (fabian.jakub@physik.uni-muenchen.de)

Abstract. The formation of shallow cumulus cloud streets was historically attributed primarily to dynamics. Here, we focus on the interaction between radiatively induced surface heterogeneities and the resulting patterns in the flow. Our results suggest that solar radiative heating has the potential to organize clouds perpendicular to the sun's incidence angle.

5 To quantify the extent of organization, we performed a high resolution LES parameter study. We varied the horizontal wind speed, the surface heat capacity, the solar zenith and azimuth angles, as well as radiative transfer parameterizations (1D and 3D). As a quantitative measure we introduce a simple algorithm that provides a scalar quantity for the degree of organization and the alignment. We find that, in the absence of a horizontal wind, 3D radiative transfer produces cloud streets per-

10 pendicular to the sun's incident direction, whereas the 1D approximation or constant surface fluxes produce circular, randomly positioned, clouds. Our reasoning for the enhancement or reduction of organization is the geometric position of the cloud's shadow and the corresponding surface fluxes. Furthermore, when increasing horizontal wind speeds to 5 or $10\,\mathrm{m\,s^{-1}}$, we observe the development of dynamically induced cloud streets. If in addition, solar radiation illuminates the surface beneath

15 the cloud, i.e. when the sun is positioned orthogonal to the mean wind field and the solar zenith angle is larger than 20°, the cloud-radiative feedback has the potential to significantly enhance the tendency to organize in cloud streets. In contrast, in the case of the 1D approximation (or overhead sun), the tendency to organize is weaker or even prohibited because the shadow is cast directly beneath the cloud. The radiative feedback on surface heterogeneities is generally diminished for large

20 surface heat capacities. We therefore expect radiative feedbacks to be strongest over land surfaces and weaker over the ocean. Given the results of this study we expect that simulations including shallow cumulus convection will have difficulties producing cloud streets if they employ 1D radiative transfer solvers or may need unrealistically high wind speeds to excite cloud street organization.

1 Introduction

25 The advent of airborne and satellite observations allow for a bird's eye view of the atmosphere and, ever since, meteorologists have been fascinated by the striped patterns often evident in cloud systems. Kuettner (1959) presented some early pictures of cloud streets from rocket and aircraft instruments. Descriptions of cloud streets, date back as far as Steinhoff (1935), who gave a detailed description of a long-distance glider flight, or Woodcock (1942) who investigated the soaring patterns of seagulls.

30 Scientific literature documenting the existence and explaining the prerequisites for the formation of cloud streets is plentiful. Weckwerth et al. (1997) and Etling and Brown (1993) provide a thorough review of past observations and theoretical frameworks. They suggest that favorable ingredients for roll vortices are weak thermal instabilities with moderate horizontal wind speeds in the planetary boundary layer.

35 Thermal instabilities are directly linked to surface fluxes and consequently to surface heterogeneities. Several studies investigated the role of surface fluxes on the development of boundary layer circulations with a focus on cloud streets. Here the literature distinguishes between static heterogeneities, i.e. differences in land-surface parameters such as vegetation, surface roughness or surface albedo and dynamic heterogeneities, such as moisture budget or temperature fluctuations.

40 Static heterogeneities in conjunction with shallow cumulus clouds and cloud streets have been examined for example by Avissar and Schmidt (1998); Patton et al. (2005); Rieck et al. (2014). In contrast, Schumann et al. (2002); Wapler (2007); Frame et al. (2009); Gronemeier et al. (2016) investigated the influence of dynamic heterogeneities in surface shading and even considered 3D radiative effects (i.e. the displacement of the shadow). However, they did not include a realistic surface

45 model, but rather adjusted the surface fluxes instantaneously. Others investigated the influence of shading coupled to an interactive surface model (Vilà-Guerau de Arellano et al., 2014; Lohou and Patton, 2014; Horn et al., 2015). However, one particularly questionable issue with those studies was the application of 1D radiative transfer solvers, which are known to introduce large spatial error in surface heating rates (O'Hirok and Gautier, 2005; Wapler and Mayer, 2008; Wissmeier et al., 2013;

50 Jakub and Mayer, 2015).

Overall, we can summarize that the formation of cloud streets has been extensively explored from theoretical and observational perspectives. The above mentioned studies shed light on the various aspects of interaction with the cloud field but either lack a realistic representation of surface processes, neglect 3D radiative transfer effects or do not examine the relationship concerning the background

55 wind speed.

In this study we strive to overcome these shortcomings and determine the prerequisites for the formation of cloud streets, while our main focus lies on dynamic heterogeneities and (3D) radiative transfer. We try to disentangle the underlying processes with a rigorous parameter study using Large-Eddy-Simulations (LES).

60 Section 2 briefly outlines the LES model, explains the setup of the simulations and introduces a

Figure 1. Virtual photograph of LES simulations at a cruising altitude of $15\,\mathrm{km}$. Top panel: cloud formation of a simulation driven by 3D radiation (TenStream with sun in the east, i.e. right ($\varphi = 90°$)). Lower-panel: cloud formation of a simulation which was performed with 1D radiation (Two-stream). The specific model setup is the same as referenced in fig. 2, i.e., no background wind and a continental land surface. The simulations differ with respect to cloud size distributions and the organization in cloud streets, the cloud fraction though is the same ($27\,\%$). The visualization was performed with a physically correct rendering with MYSTIC (MonteCarlo solver in libRadtran (Mayer, 2009; Emde et al., 2015)).

scalar metric to quantify the organization in cloud streets. In section 3 we interpret the magnitude of cloud street formations in the parameter space spanning surface properties, background wind speeds and the sun's angles. Section 4 finally summarizes key findings of the parameter study.

2 Methods and Experiments

2.1 LES Model

65

The Large-Eddy-Simulations (LES) were performed with the UCLA–LES model. A description and details of the LES model can be found in Stevens et al. (2005). The land surface model follows the implementation of the Dutch Atmospheric Large-Eddy Simulation code Heus et al. (2010). The simulations presented here use warm micro-physics formulated in Seifert and Beheng (2001) where the

70 formation of rain is turned off to prevent any further complications such as cold pool dynamics. The radiative transfer calculations are performed with the TenStream package (Jakub and Mayer, 2015), which includes a 1D Schwarzschild (thermal only), a δ-Eddington two-stream (solar and thermal), as well as the 3D TenStream (solar and thermal) solver.

The TenStream is a MPI-parallelized solver for the full 3D radiative transfer equation. In analogy

75 to a two-stream solver, the TenStream solver computes the radiative transfer coefficients for up- and

downward fluxes and additionally for sideward streams. The coupling of individual boxes leads to a linear equation system which is written as a sparse matrix and is solved using parallel iterative methods from the "Portable, Extensible Toolkit for Scientific Computation", PETSc (Balay et al., 2014) framework. In Jakub and Mayer (2015, 2016), we extensively validated the TenStream by

80   comparison with the exact Monte Carlo code *MYSTIC* (Mayer, 2009).

The most pronounced differences between 1D and 3D radiative transfer solvers, pertaining the setup here, is the displacement of the sun's shadow at the surface. In the case of 1D radiative transfer, the shadow of a cloud is by definition always directly beneath it (so called independent pixel or independent column approximation). Contrarily, 3D radiative transfer allows the propagation of

85   energy horizontally and correctly displaces the clouds shadow depending on the sun's position.

The spectral integration is performed using the correlated-k method following Fu and Liou (1992). The coupling of the TenStream solver to the UCLA–LES follows the description in Jakub and Mayer (2016). One exception is the use of the Monte-Carlo-Spectral-Integration (Pincus and Stevens, 2009) which we do not use because of limitations with regards to computations involving interactive sur-

90   face models (Pincus and Stevens, 2013).

2.2   Model Experiment Setup

The base setup of the UCLA–LES simulates a domain of $50\,\mathrm{km} \times 50\,\mathrm{km}$ with a horizontal resolution of $100\,\mathrm{m}$ and $50\,\mathrm{m}$ vertically. The simulations start from a well-mixed initial background profile with a constant virtual potential temperature ($292\,\mathrm{K}$) in the lower $700\,\mathrm{m}$ and increases by $6\,\mathrm{K\,km^{-1}}$

95   above. Water vapor near the surface amounts to $9.5\,\mathrm{g\,kg^{-1}}$, decreasing with $-1.3\,\mathrm{g\,kg^{-1}\,km^{-1}}$. The layers of the surface model are soaking wet ($30\,\%\,\mathrm{vmr}$) and stripped of vegetation with an initial temperature of $291\,\mathrm{K}$. The surface albedo for shortwave radiation is set to $7\,\%$.

The focus of this study is to determine the interplay of radiation with the atmosphere, the surface and the clouds, and finally take a closer look on the formation of cloud streets. To that end we run

100   the simulations with five free parameters, namely the heat capacity of the surface skin layer (C_{skin}), the background wind (u, i.e. west-winds), the solar zenith (θ) and azimuth (φ) angle as well as with different radiative transfer approximations (see table 1). The heat capacities are chosen to be representative for situation ranging from continental land surfaces to well mixed ocean. The coupling of radiative transfer to the land-surface model is realized in four ways. We either compute the net sur-

105   face irradiance Q_{net} with a 1D δ-eddington two-stream solver , or employ the 3D TenStream solver, with two azimuth angles. Additionally, we conducted the experiments where Q_{net} is set to a prescribed constant value (spatial and temporal average of the surface irradiance of the corresponding 1D simulation).

The time it takes the simulations to form the first clouds depends on the choice of the parame-

110   ters. Foremost the solar zenith angle determines the energy input into the atmosphere and the surface (lower positioned sun hence leads to a later onset of cloud development). To compare the het-

Table 1. Parameter space for the LES simulations: the mean west wind $\boldsymbol{u}$, the solar azimuth and zenith angle φ, θ, the surface skin heat capacity C_{skin} as a water column equivalent and three settings for the computation of net radiative surface fluxes (Q_{net}). The radiative transfer computations are done either with a 1D δ-Eddington two-stream , with the 3D TenStream solver or simulations with constant mean net irradiance. Variations of the solar azimuth φ are only applied for 3D radiative transfer. Values of Q_{net} in case of simulations without interactive radiative transfer were set to the mean surface irradiance of the 1D simulations. In total a number of 192 simulations.

$\boldsymbol{u}$	0, 5, 10	$\mathrm{m\,s^{-1}}$
φ	90, 180	°
θ	20, 40, 60, 75	°
C_{skin}	1, 10, 100, 1000	cm
Q_{net}	constant, 1D, 3D	

erogeneous simulations we limit the following analysis to the time-steps (output every $5\,\text{min}$) where the cloud fraction is between $10\,\%$ and $50\,\%$ (typical for shallow cumulus convection, e.g. Seifert and Heus (2013)). Most simulations produce clouds after about one hour and show an increase in cloud cover up to and beyond $50\,\%$ in the first $6\,\text{h}$. Simulations with low positioned sun took longer and were hence run for a longer period of $12\,\text{h}$.

Figure 1 shows a photo rendering of the LES cloud field for two simulations with differing options for the radiative transfer solver. In the top panel, 3D radiative transfer is considered with the sun positioned in the east (zenith $\theta = 60°$) and in the bottom panel panel 1D solver is applied where the shadow is by definition always cast directly beneath the clouds. In the former the organization in cloud streets perpendicular to the sun's incident angle is evident whereas the latter (1D) does not seem to organize in any way. Figure 2 presents the liquid water content and the surface heat flux for the same two simulations plus one 3D simulation where the sun is in the south. This time we look at volume rendered liquid water content and surface heat fluxes for the full domain. In figs. 1 and 2, simulations with 3D radiative transfer show organization in cloud streets with length scales of up to $20\,\text{km}$, perpendicular to the sun's incident angle. We can clearly identify these coherent cloud structures with the naked eye. However, to solidify our claims, we present a quantitative measure for the cloud distribution.

2.3 Correlation Ratio

Since we do not deal with towering and tilted or multilayer clouds we can use the cloud mask as a proxy to separate individual clouds. We derive the cloud mask as the binary field of the liquid water path (LWP > 0). We then use the normalized 2D auto correlation function of the cloud mask
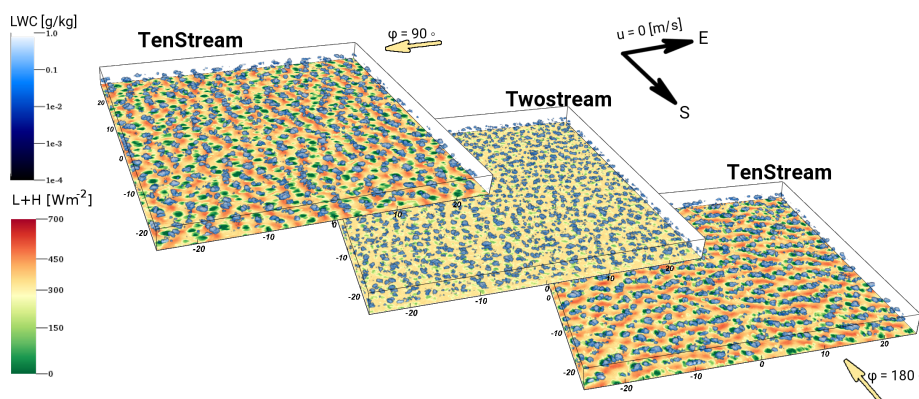
Figure 2. Volume rendered liquid water mixing ratio (LWC) and surface latent and sensible heat flux ($L + H$) for three simulations. The cloud scene of the left and mid panel have already been presented in fig. 1. In the left panel, radiative transfer calculations are performed with the TenStream solver and the sun is positioned in the east ($\varphi = 90°$). The simulation in the mid-panel is driven by a 1D two-stream solver, whereas the right panel simulation also employs the TenStream solver but the sun shining from the south ($\varphi = 180°$). The solar zenith angle is in all three simulations $\theta = 60°$, the mean background wind speed is $0\,\mathrm{m\,s^{-1}}$ and the surface skin heat capacity set to an equivalent of $1\,\mathrm{cm}$ water depth (representative for continental land surface). The snapshot shows the simulations after $3\,\mathrm{h}$ model time at a cloud fraction of $27\,\%$. Volume rendered plots were created with VISIT (Childs et al., 2012).

to analyze the spatial distribution of cloudy and clear-sky patches. The three upper panels of fig. 3 illustrate the 2D correlation coefficient for the three simulations presented in fig. 2.

Next, we use the transects of the correlation coefficient along the x- and y-axis (indicated as a black line). The lower panels in fig. 3, respectively, show the linearly interpolated linecuts of the discrete auto-correlation function. The location where the normalized correlation coefficients goes to zero defines the mean distance from a cloudy pixel where it is more likely to find a clear-sky pixel. We use the north-south and the east-west distances d_{NS} and d_{EW}, respectively, to define the correlation ratio R_{c} as:

$$R_{\mathrm{c}} = d_{\mathrm{NS}}/d_{\mathrm{EW}}$$

135   This definition would miss cloud streets in diagonal direction which, however, is no limitation for our analysis. For one, we know that the background wind induces cloud streets along track, i.e. here in the west-east component (see e.g. Weckwerth et al. (1997)). At the same time we hypothesize that radiatively induced effects will be either along or perpendicular to the incident solar beam, i.e. follow the surface inhomogeneities (see, e.g., Gronemeier et al. (2016). The two major directions
140   should therefore capture the dominant effects of dynamically and radiatively induced cloud dynamics.
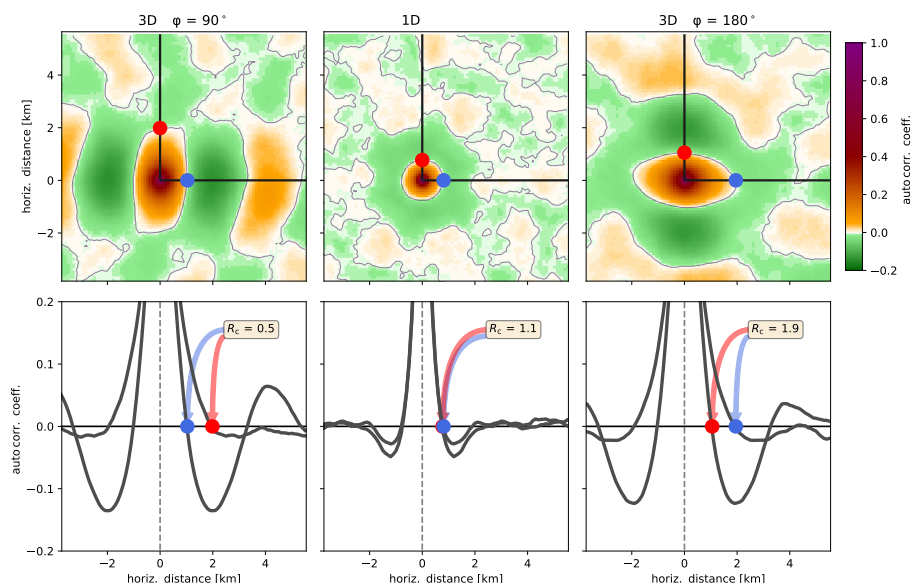
Figure 3. The panels exemplarily depict the auto-correlation coefficients of the cloud distribution in the three simulations presented in fig. 2. The upper panels show the normalized 2D autocorrelation coefficient with two intersection lines in the North-South (vertical) and the East-West (horizontal) direction. The markers pinpoint the distance in N-S (red) and E-W (blue) direction, respectively, where the auto-correlation coefficient reaches a zero value and therefore denote the distance where it becomes more likely not to find a cloud. The lower panels follow the black linecuts and further describe the two transects depicting the correlation function's root points from which we derive the correlation ratio. Simulations with 3D radiative transfer (left and right panels) shows in contrast to 1D radiative transfer (mid panel) a distinct asymmetry perpendicular to the solar incidence angle. The organization of clouds and their alignment is represented in values of the correlation ratio R_c being less than or greater than one for alignment along the y- or x-axis, respectively.

The correlation ratio reduces a cloud field snapshot into a scalar which yields $R_c = 1$ for symmetrically distributed clouds, $R_c < 1$ for organized cloud fields along the north-south direction and $R_c > 1$ if cloud features are arranged east to west. We finally compute the mean correlation ratio $\overline{R_c}$

145 as the arithmetic mean of R_c calculated at all output timesteps (every 5 minutes) where the cloud fraction is between $10\,\%$ and $50\,\%$.

3   Results and Discussion

The basis for the following analysis is the evaluation of correlation ratios as a function of the five free parameters, $\boldsymbol{u}$, φ, θ, C_{skin}, and the radiative transfer solver (for details, see table 1). Figure 4

150 shows the mean correlation ratio $\overline{R_c}$ for each of the 192 simulations. The three panels show results
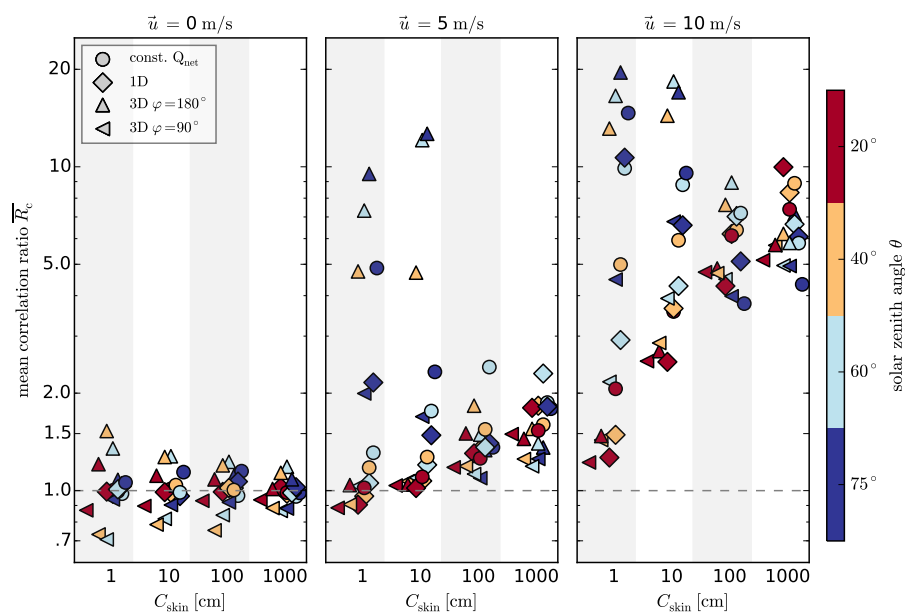
Figure 4. Correlation ratio for simulations with a variable surface skin heat capacity (C_{skin}), solar zenith angle (θ), and three wind velocities (panels left to right). Shaded areas group simulations with a constant C_{skin} according to their respective values, while the horizontal spread inside a group is merely to separate datapoints visually. Wind-component u is always from west to east while the individual markers denote simulations where the surface irradiance Q_{net} is set to a constant value, or is computed either with a 1D two-stream solver, or with the 3D TenStream where the sun is either shining from the south ($180°$) or from the east ($90°$). The correlation ratio is averaged over all timesteps where the cloud fraction is between $10\,\%$ and $50\,\%$.

for different horizontal background wind speeds, $0\,\mathrm{m\,s^{-1}}$, $5\,\mathrm{m\,s^{-1}}$ and $10\,\mathrm{m\,s^{-1}}$. Each panel's x-axis is divided into four categories for the surface skin heat capacity and the colorbar describes the solar zenith angle. Additionally, four different markers denote the various options concerning the radiative transfer solvers while the rotation of triangle markers (3D RT) denote the azimuth angle.

155   We will first focus on the left panel which shows the correlation ratios for the simulations without any background wind and later move on to simulations with wind. In other words, we start by focusing on purely radiative effects and their influence on the organization of convection and eventually add dynamically induced cloud streets to the discussion.

3.1   Without Wind: $u = 0\,\mathrm{m\,s^{-1}}$

160   The three simulations presented in section 2 are located on the far left panel of fig. 4 with a surface skin heat capacity equivalent of $1\,\mathrm{cm}$ water column (furthest to the left shaded area). Correspondingly, the markers for 3D radiative transfer are shown as triangle markers in light blue (zenith angle
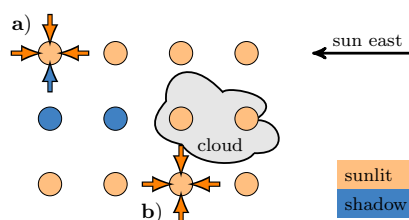
Figure 5. Sketch from an aerial view depicting surface fluxes in the vicinity of a cloud with a tilted solar incidence. The cloud casts a shadow on the westward surface pixels (blue dots). The available convective energy is directly proportional to latent and sensible heat release of the surface in the vicinity of the convective updraft. Arrows illustrate the confluence of near surface air masses from adjacent pixels in a thermally driven updraft event. Convective tendencies will be weaker on pixels that are adjacent to shaded patches, e.g. at a). In contrast, pixels that are surrounded by sun-lit patches, e.g. b), are likely to show enhanced convective motion. This pattern favors the organization of cumulus convection in stripes perpendicular to the sun's incident.

of 60°). The upward triangle represents the sun positioned in the south and yields a mean correlation ratio of 1.5 (rolls produced west to east). In contrast, the left rotated triangle presents a sun positioned in the east and shows a mean correlation ratio of .7 (rolls produced south to north). The simulation with 1D radiative transfer is presented with a diamond shaped marker and shows a mean correlation ratio of ≈ 1 (no organization).

To explain the concept of why 3D RT creates rolls, we may setup a quick thought experiment. First start with the assumption that there already is a single cloud which will cast the shadow along the sun's incident angle. The surface fluxes for latent sensible heat will be smaller in the shadowy area and hence we expect the next convective plume to rise in sun-lit areas. Figure 5 illustrates the concept for a single cloud and the resulting pattern for surface fluxes. The schematic only constrains convection to be less favorable on the shadowy side but it does not necessarily favor the perpendicular directions over the direction towards the sun. However, if a cloud would evolve on the sun-facing side, the resulting shadow would in turn lead to a faster dissipation of the initial cloud and is thereby an unstable environment for persistent cloud patterns. Following this, we expect the convection to occur favorably perpendicular to the sun's incident angle purely from geometric reasoning.

It is also clear from the horizontal axis of fig. 4 that higher heat capacities lead to less pronounced formations of cloud streets which is to be expected because it weakens the radiative impact and consequently reduces the dynamically induced surface heterogeneities. Yet, though weaker, we still find an impact in 3D radiative transfer simulations even for a water column equivalent of $10\,\mathrm{m}$. In this case with such high surface heat capacities, the simulation do not exhibit any variability in surface fluxes and radiation solely acts through atmospheric heating. We recover this behavior also in simulations with a fixed sea surface temperature or with constant latent and sensible surface

185 fluxes (not shown). In Jakub (2016, fig. 3.22), we show that the asymmetric heating of the cloud
   sides (or similarly in Wapler (2007); Gronemeier et al. (2016) for displaced surface shadows) intro-
   duces a secondary circulation by lifting the sun-lit side and enhancing subsidence on the shadowy
   side. This asymmetry introduces a wind shear component consisting of a horizontal wind away from
   the sun at cloud height and towards the sun near the surface. Given that the effects of atmospheric
190 heating is much smaller and happens on longer timescales compared to the surface feedback we put
   the interpretation aside for another time.

   Simulations with one-dimensional radiative transfer or constant Q_{net} do not produce cloud streets
   which is reflected by correlation ratios $R_{\mathrm{c}} \approx 1$. If we apply the same geometric reasoning from fig. 5
   for these simulations, where the shadow is either directly beneath the cloud or with no heterogeneity
195 at all, it is clear that there can be no preferential direction for convective organization.

   Three-dimensional radiation calculations with high or low solar zenith angles also show a reduced
   production of cloud streets. This is, (a) because low zenith angles (sun above head) practically be-
   have just as 1D radiative transfer, and (b), because large zenith angles (low sun, smaller heating rates)
   have a weaker potential to create surface heterogeneities.

200 **3.2 Medium Wind: $u = 5\,\mathrm{m\,s}^{-1}$**

   The middle panel of fig. 4 presents the correlation ratios for simulations with a horizontal back-
   ground wind of $5\,\mathrm{m\,s}^{-1}$. If we first shift our attention to the simulations with constant surface irra-
   diance Q_{net} (round markers), it is evident that the introduction of a mean wind profile leads to the
   formation of cloud streets ($\overline{R}_{\mathrm{c}} > 1$), irrespective of radiatively induced surface heterogeneities. This
205 is consistent with the literature on the formation of cloud streets which was introduced in section 1.
   Interestingly, we find a spread in the development of cloud streets depending on the magnitude of
   the prescribed Q_{net}, with correlation ratio ranging from 1 to 5. While thermally driven convection in
   conjunction with a vertical wind shear is a key ingredient for the formation of cloud streets, we find
   less pronounced organization in cases with high surface fluxes. This may be explained following the
210 remark of Weckwerth et al. (1997): "*...rolls are most commonly observed within slightly unstable
   environments. As the convective boundary layer becomes more unstable it is generally expected that
   growth of two-dimensional convective instabilities is less preferred.*"

   Strong radiative heating, such as we get for high sun (i.e. small θ) results in an increased atmospheric
   instability. Fully quantifying the intricate relation between thermal instabilities and the formation of
215 cloud streets is an endeavor in itself and to the best of our knowledge, there is not yet a definitive
   answer. Anyway, from our results, it is evident that a medium background wind profile dynamically
   induces cloud street organization with correlation ratios on the order of $R_{\mathrm{c}} \approx 1.5$.

   So far we discussed only the simulations with constant Q_{net}. When we look at land surfaces that
   are coupled to radiative transfer calculations (1D and 3D markers in fig. 4), we find that radiative
220 heating may either enhance the organization ($\overline{R}_{\mathrm{c}}$ up to 13) or counter-act it ($\overline{R}_{\mathrm{c}} < 1$). The following

paragraph examines the superposition of dynamically and radiatively induced tendencies to organize the clouds.

Let's consider the case that there is a dynamically induced cloud street along the mean background wind, i.e. from west to east. Quasi 1D radiation (1D and 3D if sun is close to zenith) casts a shadow onto the cloud's updraft region and therefore hinders further development of the cloud. This results in values for the correlation ratio of $\overline{R}_c \approx 1$. Similarily, 3D radiation where the azimuth is in the same direction as the wind (here east, $\varphi = 90°$, left-rotated markers) also inhibits the formation of cloud streets or may even oppose the dynamically induced organization and produce correlation ratios $\overline{R}_c < 1$.

In contrast, for 3D radiative transfer with solar incidence perpendicular to the mean wind, i.e. sun from south or north, and permitted that the sun's zenith angle allows to illuminate the surface beneath the cloud ($\theta > 20°$), we find that the radiative tendency to organize the clouds amplifies the dynamically one. This synergistic behaviour results in correlation ratios $\overline{R}_c$ between 5 and 13.

As mentioned previously in section 3.1, we again find a generally diminished influence of surface radiative heating in simulations with larger surface heat capacities.

3.3 Strong Wind: $u = 10\,\mathrm{m\,s^{-1}}$

A stronger background wind profile of $10\,\mathrm{m\,s^{-1}}$ principally shows similar behavior as the case that was presented with medium wind speeds (see right panel of fig. 4). The mean correlation ratios of purely dynamically induced cloud streets (simulations with constant Q_{net}, i.e. circle markers) cover an increasingly large range of ratios from 2 to 14. Strong solar radiation coupled with small surface heat capacities still manage to efficiently suppress the formation of cloud streets (i.e. $\overline{R}_c$ consistently smaller than purely dynamic values). Whereas illumination perpendicular to the wind direction ($\varphi = 180$ and $\theta > 20°$) again greatly amplifies the occurrence of cloud streets. This might be surprising if we consider that horizontal wind should indeed smooth out the impact of radiative surface heating. Lohou and Patton (2014) for example also suggest that wind speeds of $10\,\mathrm{m\,s^{-1}}$ may decouple the effects of dynamically induced surface heterogeneities from the evolution of clouds. However, if we consider that the dynamically induced cloud streets have typical length scales of $50\,\mathrm{km}$ (Kuettner, 1959), then, as far as radiative heating at the surface is concerned, the cloud appears to be standing still. In other words, when a dynamically induced cloud feature aligns in such a way that it persistently shades a surface region for an extended period of time, we expect that the surface heterogeneities due to radiative transfer in turn interact with the flow. It is this intricate linkage between dynamically induced cloud structures and (3D) radiative transfer that may enable or prohibit the formation of cloud streets.

4 Summary & Conclusions

255 The formation of cumulus cloud streets was historically attributed primarily to dynamics. This work aims to document and quantify the generation of radiatively induced cloud street structures. To that end we performed 192 LES simulations with varying parameters (see table 1) for the horizontal wind speed, the surface heat capacity, the solar zenith and azimuth angle, as well as for different radiative transfer solvers (section 2.2). As a quantitative measure for the development of cloud streets, we

260 introduce a simple algorithm using the autocorrelation function on the cloud mask (section 2.3), which provides a scalar quantity for the degree of organization in cloud streets and the alignment along the cardinal directions.

We find that, in the absence of a horizontal wind, 3D radiative transfer produces cloud streets perpendicular to the sun's incident direction whereas the 1D approximation or constant surface ir-

265 radiance produce circular, randomly positioned, clouds. Our reasoning for this is the geometric position of the cloud's shadow and the corresponding feedback on surface fluxes which enhances or diminishes convective tendencies (see fig. 5 for details). While the data indicates that there exists an influence due to atmospheric heating rates, we find that the differences between 1D and 3D radiation stem predominantly from surface heating, i.e. the horizontal displacement of cloud shadows.

270 Furthermore, with increasing horizontal wind speeds of 5 or $10\,\mathrm{m\,s^{-1}}$, we observe the development of dynamically induced cloud streets. So far, this is consistent with the literature on the formation of cloud streets which is introduced in section 1.

However, if solar radiation illuminates the surface beneath the cloud, i.e. when the sun is positioned orthogonal to the mean wind field and the solar zenith angle is larger than $20°$, the cloud-

275 radiative feedback may significantly enhance the tendency to organize in cloud streets. In contrast, in the case of the 1D approximation (or also 3D if the sun is aligned with the mean wind), the tendency to organize in cloud streets is weaker or even prohibited because the shadow is cast directly beneath the cloud, weakening the cloud's updraft. The radiative feedback on surface heterogeneities is generally diminished for large surface heat capacities. We therefore expect radiative feedbacks to

280 be strongest over land surfaces and less so over the ocean. Given the results of this study we expect that simulations including shallow cumulus convection will have difficulties to produce cloud streets if they employ 1D radiative transfer solvers or, may need unrealistically high wind speeds to excite cloud street organization.

Future studies have to examine if the relationship between radiative transfer and convective cloud

285 streets also applies to the real world with all the complexities of static surface heterogeneities and complex wind fields. A promising start is an analysis of the simulations within the HDCP[2] project (Heinze et al., 2017) which will allow us to test the here proposed interpretations in a more realistic setup.

Acknowledgements. This work was funded by the Federal Ministry of Education and Research (BMBF) through the High Definition Clouds and Precipitation for Climate Prediction (HD(CP)2) project (FKZ: 01LK1208A,
01LK1507D). Many thanks to Cathy Hohenegger, Bjorn Stevens and the DKRZ, Hamburg for fruitful discussions and for providing us with the computational resources to conduct our studies. Special thanks also to Alois Dirnaichner who improved this manuscript by thoroughly proofreading.

References

Avissar, R. and Schmidt, T.: An evaluation of the scale at which ground-surface heat flux patchiness affects
the convective boundary layer using large-eddy simulations, Journal of the Atmospheric Sciences, 55, 2666–
2689, doi:10.1175/1520-0469(1998)055<2666:AEOTSA>2.0.CO;2, 1998.

Balay, S., Abhyankar, S., Adams, M. F., Brown, J., Brune, P., Buschelman, K., Eijkhout, V., Gropp, W. D.,
Kaushik, D., Knepley, M. G., McInnes, L. C., Rupp, K., Smith, B. F., and Zhang, H.: PETSc Users Manual,
Tech. Rep. ANL-95/11 - Revision 3.5, Argonne National Laboratory, 2014.

Childs, H., Brugger, E., Whitlock, B., Meredith, J., Ahern, S., Pugmire, D., Biagas, K., Miller, M., Harrison, C.,
Weber, G. H., Krishnan, H., Fogal, T., Sanderson, A., Garth, C., Bethel, E. W., Camp, D., Rübel, O., Durant,
M., Favre, J. M., and Navrátil, P.: VisIt: An End-User Tool For Visualizing and Analyzing Very Large Data,
in: High Performance Visualization–Enabling Extreme-Scale Scientific Insight, pp. 357–372, 2012.

Emde, C., Buras-Schnell, R., Kylling, A., Mayer, B., Gasteiger, J., Hamann, U., Kylling, J., Richter, B., Pause,
C., Dowling, T., et al.: The libRadtran software package for radiative transfer calculations (Version 2.0),
Geoscientific Model Development Discussions, 8, 10 237–10 303, doi:10.5194/gmd-9-1647-2016, 2015.

Etling, D. and Brown, R.: Roll vortices in the planetary boundary layer: A review, Boundary-Layer Meteorol-
ogy, 65, 215–248, doi:10.1007/BF00705527, 1993.

Frame, J. W., Petters, J. L., Markowski, P. M., and Harrington, J. Y.: An application of the tilted in-
dependent pixel approximation to cumulonimbus environments, Atmospheric Research, 91, 127–136,
doi:10.1016/j.atmosres.2008.05.005, 2009.

Fu, Q. and Liou, K.: On the correlated k-distribution method for radiative transfer in nonho-
mogeneous atmospheres, Journal of the Atmospheric Sciences, 49, 2139–2156, doi:10.1175/1520-
0469(1992)049<2139:OTCDMF>2.0.CO;2, 1992.

Gronemeier, T., Kanani-Sühring, F., and Raasch, S.: Do Shallow Cumulus Clouds have the Potential to Trigger
Secondary Circulations Via Shading?, Boundary-Layer Meteorology, pp. 1–27, doi:10.1007/s10546-016-
0180-7, 2016.

Heinze, R., Dipankar, A., Henken, C. C., Moseley, C., Sourdeval, O., Trömel, S., Xie, X., Adamidis, P., Ament,
F., Baars, H., Barthlott, C., Behrendt, A., Blahak, U., Bley, S., Brdar, S., Brueck, M., Crewell, S., Deneke, H.,
Di Girolamo, P., Evaristo, R., Fischer, J., Frank, C., Friederichs, P., Göcke, T., Gorges, K., Hande, L., Hanke,
M., Hansen, A., Hege, H.-C., Hoose, C., Jahns, T., Kalthoff, N., Klocke, D., Kneifel, S., Knippertz, P., Kuhn,
A., van Laar, T., Macke, A., Maurer, V., Mayer, B., Meyer, C. I., Muppa, S. K., Neggers, R. A. J., Orlandi,
E., Pantillon, F., Pospichal, B., Röber, N., Scheck, L., Seifert, A., Seifert, P., Senf, F., Siligam, P., Simmer,
C., Steinke, S., Stevens, B., Wapler, K., Weniger, M., Wulfmeyer, V., Zängl, G., Zhang, D., and Quaas, J.:
Large-eddy simulations over Germany using ICON: a comprehensive evaluation, Quarterly Journal of the
Royal Meteorological Society, 143, 69–100, doi:10.1002/qj.2947, http://dx.doi.org/10.1002/qj.2947, 2017.

Heus, T., Van Heerwaarden, C., Jonker, H., Pier Siebesma, A., Axelsen, S., Dries, K., Geoffroy, O., Moene, A.,
Pino, D., De Roode, S., et al.: Formulation of the Dutch Atmospheric Large-Eddy Simulation (DALES) and
overview of its applications, Geoscientific Model Development, 3, 415–444, doi:10.5194/gmd-3-415-2010,
2010.

Horn, G., Ouwersloot, H., De Arellano, J. V.-G., and Sikma, M.: Cloud Shading Effects on Characteristic Boundary-Layer Length Scales, Boundary-Layer Meteorology, 157, 237–263, doi:10.1007/s10546-015-0054-4, 2015.

Jakub, F.: On the impact of three dimensional radiative transfer on cloud evolution, http://nbn-resolving.de/urn:nbn:de:bvb:19-197226, 2016.

Jakub, F. and Mayer, B.: A three-dimensional parallel radiative transfer model for atmospheric heating rates for use in cloud resolving models—The TenStream solver, Journal of Quantitative Spectroscopy and Radiative Transfer, pp. –, doi:http://dx.doi.org/10.1016/j.jqsrt.2015.05.003, http://www.sciencedirect.com/science/article/pii/S0022407315001727, 2015.

Jakub, F. and Mayer, B.: 3-D radiative transfer in large-eddy simulations–experiences coupling the TenStream solver to the UCLA-LES, Geoscientific Model Development, 9, 1413–1422, doi:10.5194/gmd-9-1413-2016, 2016.

Kuettner, J.: The Band Structure of the Atmosphere, Tellus, 11, 267–294, doi:10.3402/tellusa.v11i3.9319, 1959.

Lohou, F. and Patton, E. G.: Surface energy balance and buoyancy response to shallow cumulus shading, Journal of the Atmospheric Sciences, 71, 665–682, doi:10.1175/JAS-D-13-0145.1, 2014.

Mayer, B.: Radiative transfer in the cloudy atmosphere, in: EPJ Web of Conferences, vol. 1, pp. 75–99, EDP Sciences, doi:10.1140/epjconf/e2009-00912-1, 2009.

O'Hirok, W. and Gautier, C.: The impact of model resolution on differences between independent column approximation and Monte Carlo estimates of shortwave surface irradiance and atmospheric heating rate., Journal of the atmospheric sciences, 62, doi:10.1175/JAS3519.1, 2005.

Patton, E. G., Sullivan, P. P., and Moeng, C.-H.: The influence of idealized heterogeneity on wet and dry planetary boundary layers coupled to the land surface, Journal of the Atmospheric Sciences, 62, 2078–2097, doi:10.1175/JAS3465.1, 2005.

Pincus, R. and Stevens, B.: Monte Carlo spectral integration: A consistent approximation for radiative transfer in large eddy simulations, Journal of Advances in Modeling Earth Systems, 1, doi:10.3894/JAMES.2009.1.1, 2009.

Pincus, R. and Stevens, B.: Paths to accuracy for radiation parameterizations in atmospheric models, Journal of Advances in Modeling Earth Systems, 5, 225–233, doi:10.1002/jame.20027, 2013.

Rieck, M., Hohenegger, C., and van Heerwaarden, C. C.: The influence of land surface heterogeneities on cloud size development, Monthly Weather Review, 142, 3830–3846, doi:10.1175/MWR-D-13-00354.1, 2014.

Schumann, U., Dörnbrack, A., and Mayer, B.: Cloud-shadow effects on the structure of the convective boundary layer, Meteorologische Zeitschrift, 11, 285–294, doi:10.1127/0941-2948/2002/0011-0285, 2002.

Seifert, A. and Beheng, K. D.: A double-moment parameterization for simulating autoconversion, accretion and selfcollection, Atmospheric research, 59, 265–281, doi:10.1016/S0169-8095(01)00126-0, 2001.

Seifert, A. and Heus, T.: Large-eddy simulation of organized precipitating trade wind cumulus clouds, Atmospheric Chemistry and Physics, 13, 5631–5645, doi:10.5194/acp-13-5631-2013, 2013.

Steinhoff, E.: Excerpt from flight report on the first glider flight in cloud-streets, Tellus, 11, 267–294, doi:10.3402/tellusa.v11i3.9319, excerpt is attached in the Appendix of J. Kuettner, 1959, The Band Structure of the Atmosphere, 1935.

370   Stevens, B., Moeng, C.-H., Ackerman, A. S., Bretherton, C. S., Chlond, A., de Roode, S., Edwards, J., Golaz, J.-C., Jiang, H., Khairoutdinov, M., et al.: Evaluation of large-eddy simulations via observations of nocturnal marine stratocumulus, Monthly weather review, 133, 1443–1462, doi:10.1175/MWR2930.1, 2005.

Vilà-Guerau de Arellano, J., Ouwersloot, H. G., Baldocchi, D., and Jacobs, C. M.: Shallow cumulus rooted in photosynthesis, Geophysical Research Letters, 41, 1796–1802, doi:10.1002/2014GL059279, 2014.

375   Wapler, K.: Der Einfluss des dreidimensionalen Strahlungstransportes auf Wolkenbildung und -entwicklung, http://nbn-resolving.de/urn:nbn:de:bvb:19-68948, 2007.

Wapler, K. and Mayer, B.: A Fast Three-Dimensional Approximation for the Calculation of Surface Irradiance in Large-Eddy Simulation Models., Journal of Applied Meteorology & Climatology, 47, doi:10.1175/2008JAMC1842.1, 2008.

380   Weckwerth, T. M., Wilson, J. W., Wakimoto, R. M., and Crook, N. A.: Horizontal convective rolls: Determining the environmental conditions supporting their existence and characteristics, Monthly weather review, 125, 505–526, doi:10.1175/1520-0493(1997)125<0505:HCRDTE>2.0.CO;2, 1997.

Wissmeier, U., Buras, R., and Mayer, B.: paNTICA: A Fast 3D Radiative Transfer Scheme to Calculate Surface Solar Irradiance for NWP and LES Models., Journal of Applied Meteorology & Climatology, 52,
385   doi:10.1175/JAMC-D-12-0227.1, 2013.

Woodcock, A. H.: Soaring over the Open Sea, The Scientific Monthly, 55, 226–232, 1942.